Journal of Molecular Liquids 298 (2020) 112019

Contents lists available at ScienceDirect

Journal of Molecular Liquids

journal homepage: www.elsevier.com/locate/molliq

Incorporation of cyclodiene pesticides and their polar metabolites to model membranes of soil bacteria

Aneta Wójcik [a], Paulina Perczyk [a], Paweł Wydro [b], Marcin Broniatowski [a,*]

[a] Department of Environmental Chemistry, Faculty of Chemistry, Jagiellonian University, Gronostajowa 2, 30-387, Kraków, Poland
[b] Department of Physical Chemistry and Electrochemistry, Faculty of Chemistry, Jagiellonian University, Gronostajowa 2, 30-38, Kraków, Poland

ARTICLE INFO

Article history:
Received 12 September 2019
Received in revised form 22 October 2019
Accepted 25 October 2019
Available online 2 November 2019

ABSTRACT

The world-wide application of cyclodiene pesticides (CP) lead to severe pollution of arable land and because of the long half-lives they will be for many decades present in the soil. The only reasonable way of the elimination of these chemicals from the soil is bioremediation – the introduction to the soil of decomposer microorganisms strains capable of CP degradation. CP are highly hydrophobic and exhibit large membrane activity; thus, they can be incorporated to the cellular membrane and retained therein. The presence of CP and their metabolites in the cellular membrane of the decomposer organism can lead to severe alterations of its function and in consequence to the death of the decomposer cell. Microorganisms protect themselves changing the phospholipid composition of their membranes. To shed light on the correlation between the membrane composition and its interactions with CP and their metabolites we applied Langmuir monolayers as versatile models of decomposers' membranes. By the proper selection of phospholipids we prepared different models of cellular membranes of Gram-negative and Gram-positive bacteria. The model membranes were doped by four most frequently applied CP and their common metabolite. The combined application of microscopic, diffractometric and spectroscopic methods proved that CP can be incorporated into the model membranes and that the membrane activity of endosulfan is comparable with endrin – one of the most toxic pesticides. The penetration tests and spectroscopic studies proved also the possibility of the uptake of the polar CP metabolites by the model membranes from the aqueous subphase.

1. Introduction

Polychlorinated cyclodiene pesticides (CP) were introduced at the American market at the early fifties of the XX century as successors and complements to DDT widely applied in that times [1–6]. The application spectrum of CP was very wide ranging from insecticidal via acaricidal to rodenticidal or even avicidal [7]. It was soon realized that even low doses of CP lead to chronic intoxication of the non-target organisms including human because of their accumulation in the animal adipose tissue [8]. Moreover, it was also proved that 60% or even more of the applied CP dose accumulates in the soil [9,10], which is connected with the long half-life times of CP, being 25 years for aldrin or even longer for other CP [3]. Due to their extraordinary toxicity, accumulation in the environment and bioaccumulation in animal tissues most of the CP were banned in the USA at the beginning of the seventies of the previous century [11]. However, in the developing countries they were applied much longer, even to the 2000 year. CP are classical examples of persistent organic pollutants (POP) [12] and as such were included to the first protocol A, the so-called dirty dozen list, of the Stockholm Convention – an international legal act regarding POP acquired in the year 2001 [13,14]. CP were banned in most countries but because of their long half-life times they are still detected in multiple contaminated sites. What is interesting, endosulfan, also produced from hexachlorocyclopentadiene, was considered much less toxic than the other CP; thus it was produced annually in the amount of 50000 tones and applied globally, especially in developing countries as India, China and South American and African countries [15]. Finally, endosulfan was added to the protocol A of Stockholm convention and in 2011 banned in India, but due to its vast applications multiple areas were severely polluted by this pesticide. Moreover, there are still some developing countries in Africa and Asia using this pesticide [15]. The most powerful method of POP elimination from polluted soil is biodegradation, that is bacteria or fungi lead decomposition of POP to nontoxic and preferably inorganic products [16,17]. It was proved that multiple bacterial strains could use endoslufan as the sole carbon and/or sulfur source [18–21]. However, such studies were performed mainly in laboratories; whereas, in real field conditions the application of endoslufan to the soil lead to profound impoverishment of decomposer organisms and the disappearance of whole genera of bacteria and fungi [22–25]. In anaerobic conditions bacteria detach the sulfur atom from endosulfan converting this compound to endosulfan diol and finally upon further

* Corresponding author.
E-mail address: broniato@chemia.uj.edu.pl (M. Broniatowski).

https://doi.org/10.1016/j.molliq.2019.112019

oxidation to chlorendic acid [26]. The problem is that no of the six chlorine atoms is cleaved in such biodegradation and that the degradation products are the same for endosulfan and the dirty-dozen CP as aldrin or endrin [27]. The other, even more significant problem, is the water solubility of chlorendic acid which enables its migration in surface and ground waters at far distances from the original pollution source [26,28]. It was corroborated by multiple publications that the toxicity to the non-target vertebrata as well as to the soil decomposer microorganisms is strictly connected with the membrane activity of CP [29]. Indeed, CP are lipophilic which founds its manifestation in high water/octanol partition coefficient values [30]. The incorporation of CP into the phospholipid matrix leads to profound alterations in the membrane organization, affects the phospholipid-protein interactions, induces membrane protein misfolding and finally triggers the metabolic cascades leading to the death of the soil microorganism [29,31]. Microorganisms can adapt to the harsh, polluted environment by adjusting the phospholipid composition of the membrane, which consists in changing the mutual proportion of the main phospholipid classes and/or the length and structure of hydrophobic moieties of these molecules [32,33]. The microorganisms intended for applications in the bioremediation of CP polluted soils should be especially durable to the membrane-destructive action of these pesticides. On the other hand the phospholipid composition of the cellular membrane of the microorganisms applied in POP biodegradation can be affected and deliberately altered by the application of selected surfactants [34–36] or natural xenobiotics [37] provided simultaneously with fertilizers to the remediated land. However, to preform such procedures effectively the correlation between the membrane composition and its susceptibility to CP incorporation should be known. Due to the complexity of the discussed here phenomena the application of model membranes of simplified, well-known and adjustable phospholipid composition imitating the real microbial membranes can lead to progress in this research field.

Therefore, to shed light on these phenomena, crucially important for effective remediation of the polluted land, we applied model systems emulating the phospholipid membranes. In our studies, as the models of bacterial membranes we applied Langmuir monolayers composed of phospholipids typically found in bacterial membranes. Soil bacteria belong both to the Gram-negative and Gram-positive groups; that is differ significantly in the composition of the phospholipid matrix. Thus, in our studies we modeled the membranes of the both vast groups of soil bacteria. In the inner membranes of Gram-negative bacteria the zwitterionic phosphatidylethanolamines (PE) dominate over the anionic phospholipids: phosphatidylglycerols (PG) and cardiolipin (CL) constituting 70–80% of all phospholipids [38,39]. On the contrary, in the membranes of Gram-positive bacteria the anionic phospholipids significantly dominate over the PE [38,40]. In this aspect the Gram-positive bacteria can be divided onto two groups: these in which PE is detected at the level of ca. 20–30% and these virtually devoid of zwitterionic phospholipids, the membrane of which are composed practically solely of PG and CL [32,41]. In our studies we prepared model systems to emulate all these cases. Four different CP were applied: endosulfan (EDS), because of its vast past and present applications and problems with its biodegradation and three CP from the "dirty dozen": aldrin (ALD), endrin (END) and mirex (MX). The last three pesticides were banned in most countries several decades ago, but due to their long half-lives they are and for long will be detected on high levels in multiple contaminated sites, so their biodegradation is still an unresolved problem. CP pose danger to soil decomposer microorganisms not only in their original form, as their polar water soluble metabolites, as for example chlorendic acid (CHA), can be even more toxic to them. Therefore, in our studies the effects of CHA on the model membranes were also investigated. In our studies we applied the Langmuir technique, that is the registration of the surface pressure (π) – mean molecular area (A) isotherms upon the monolayer compression. The texture of the model membranes was visualized in the mesoscopic micrometer scale with the application of Brewster angle microscopy (BAM), whereas the structure of the membranes in the molecular Ångstrom scale was investigated with the application of Grazing incidence X-ray diffraction (GIXD). The effects exerted by the adsorption of CHA from aqueous solution on the organization of the model membrane and especially on the conformation of the phospholipid polar head-group was studied with the application of the surface specific Polarization Modulated Infrared Reflection Absorption Spectroscopy (PM-IRRAS).

2. Experimental

2.1. Materials

The applied phospholipids: 1,2-dimyristoyl-*sn*-glycero-3-phosphoethanolamine (DMPE), 1,2-dimyristoyl-*sn*-glycero-3-phospho-(1′-rac-glycerol) (sodium salt) (DMPG) and 1′,3′-bis[1,2-dimyristoyl-*sn*-glycero-3-phospho]-glycerol (sodium salt) (TMCL) were purchased from Avanti Polar Lipids as lyophilized powders of the purity 99%. The samples were sent with dry ice and were stored refrigerated at −20 °C. Spectroscopic grade chloroform (99.9%) stabilized by ethanol, spectroscopic grade methanol (99.9%) and ethanol (98%, pure per analysis) were purchased from Sigma-Aldrich. The investigated cyclodiene pesticides: endosulfan (EDS), aldrin (ALD), endrin (END), mirex (MX) and chlorendic acid (CHA) were purchased also from Sigma-Aldrich, as analytical standards of the purity > 99%. The structural formulae of the investigated CP are shown in Scheme 1. The ultrapure water of the resistivity of 18.2 MΩ cm was produced in the laboratory with the application of Merck-Millipore Synergy12 water-purification system.

2.2. Solutions and membrane models

Samples of the phospholipids and pesticides were weighted on Mettler Toledo semi-micro balance with the accuracy of 10 μg. The typical weight of the phospholipid sample was close to 2.5 mg and of CP around 1–1.5 mg. The samples were dissolved in 10 cm^3 volumetric flasks in chloroform/methanol (9/1 v/v) mixture. The concentrations of DMPE and DMPG were close to 0.4 mM, of TMCL to 0.2 mM and the concentrations of the pesticides were ca. 0.25–0.4 mM, depending on the sample. The stock solutions were kept refrigerated at −20 °C.

The proper volumes of the phospholipid stock solutions were mixed in 5 cm^3 volumetric flasks to achieve the required mole proportions of the phospholipid molecules. 6 model systems were prepared: GNC and GNG emulating Gram-negative bacteria membranes, GPC and GPG emulating Gram-positive bacterial membranes, BAC and BAG emulating the membranes of Gram-positive bacteria devoid of zwitterionic phospholipids. The compositions of these model membranes are presented in Table 1.

Appropriate volumes of the binary phospholipid solutions were mixed just before experiments in amber glass vials with the stock solutions of the pesticides to achieve the mole ratio of the pesticide X(CP) = 0.1 and 0.3.

0.05 M solution of chlorendic acid in ethanol was prepared and used in the penetration experiments. CHA is quite well soluble in water but much higher concentrations can be achieved in ethanol. In the penetration tests we intended to achieve the final CHA concentration in the subphase of 10^{-4} M with the minimal change of the subphase volume after the injection of CHA solution. Therefore the application of the concentrated ethanol solution was here preferable.

2.3. Techniques

Two identical KSV-NIMA double-barrier Langmuir-Blodgett troughs, model KN2002 of the nominal area of 275 cm^2 were applied for the registration of the π-A isotherms, penetration tests and PM-IRRAS experiments. These troughs had a rectangular deposition well located centrally and were fabricated from a single block of Teflon without

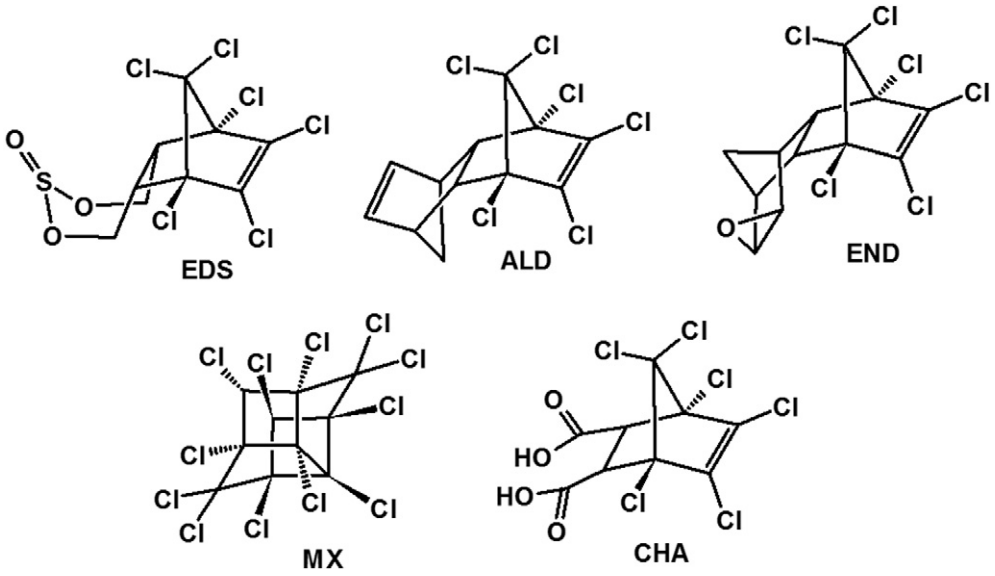

Scheme 1. Structural formulae of the investigated cyclodiene pesticides.

any glued elements. In the BAM experiments a larger double barrier KSV-NIMA LB trough (KN 1006) of the area of 841 cm^2 was used. The GIXD experiments were performed on a custom-ordered Riegler&Kirstein (R&K) single barrier Langmuir trough of the area of approx. 500 cm^2. The management of the troughs was identical in all the experiments. After each experiment the monolayer material was removed from the surface with a vacuum aspirator, after which the whole aqueous subphase was removed. The trough was cleaned with a fiberless tissue soaked in chloroform which was followed with a tissue soaked in isopropanol, after which the trough was rinsed with plentiful of ultrapure water. The clean trough was filled with ultrapure water which was used as the subphase in all the experiments. The required volume of the phospholipid chloroform solution was deposited dropwise at the water/air interface with the application of Hamilton analytical syringes. 10 min were left for chloroform evaporation after which the monolayers were compressed with the rate of 20 $cm^2\ min^{-1}\cdot molecule^{-1}$ and the π-A isotherms were registered. Surface pressure was measured with a Wilhelmy tensiometer (KSV NIMA) applying a rectangular plate of filtration paper (Whatman ashless) as the surface pressure sensor. The accuracy of the surface pressure measurement was 0.05 mN/m; whereas the uncertainty of the mean molecular area (A) was ± 1 $Å^2$/molecule. Each π-A isotherm was registered three times in separate experiments. All the measurements were performed at 20 °C and the temperature of the aqueous subphase was kept constant with the application of Julabo water-circulating bath.

Compression modulus, C_S^{-1} was calculated from the π-A isotherms according to its definition [42]:

$$C_S^{-1} = -A\left(\frac{\partial \pi}{\partial A}\right)_T, p, n$$

where the indices T, p and n indicate the constant temperature, pressure and composition of the monolayer, respectively.

In the penetration tests the monolayers were compressed to the required surface pressure of 10, 20 or 30 mN/m, after which the mean molecular area was kept constant. 20 min. were left for monolayer stabilization after which 500 μl of the 0.05 M CHA solution in ethanol was injected via the injection port deep into the well of the Langmuir trough. The subphase in the well was mixed with a magnetic stirrer to facilitate the diffusion of CHA in the subphase. After the injection the temporal evolution of the surface pressure value was monitored by at least 1 h. In a blank experiment 500 μl of ethanol was injected to the subphase and it was proved that such an amount of this solvent had no effect on the measured surface pressure values.

2.4. Brewster angle microscopy (BAM)

UltraBAM instrument (Accurion GmbH, Goettingen, Germany) equipped with a 50 mW laser emitting p-polarized light at a wavelength of 658 nm, a 10x magnification objective, polarizer, analyzer and a CCD camera was used. The spatial resolution of the microscope was 2 μm. The foregoing apparatus and the Langmuir trough were placed on the table (Standa Ltd, Vilnius, Lithuania) equipped with active vibration isolation system (antivibration system VarioBasic 40, Halcyonics, Göttingen, Germany).

2.5. Grazing incidence X-ray diffraction (GIXD)

The experiments were performed on the SIRIUS beamline at SOLEIL synchrotron (Gif-sur- Yvette, France) using the dedicated liquid surface diffractometer. The detailed construction of the diffractometer working at the SIRIUS beamline and the parameters of the synchrotron beam

Table 1

Mole ratios of the phospholipid components of the model membranes. X(i) – mole ratio of the ith component is defined as follows: $X(i) = \frac{N_i}{\sum_1^n N_i}$ where N_i is the number of molecules of the ith component and n is the number of components.

model	X(DMPE)	X(DMPG)	X(TMCL)
GNC	0.7	–	0.3
GNG	0.7	0.3	–
GPC	0.2	–	0.8
GPG	0.2	0.8	–
BAC	–	0.25	0.75
BAG	–	0.75	0.25

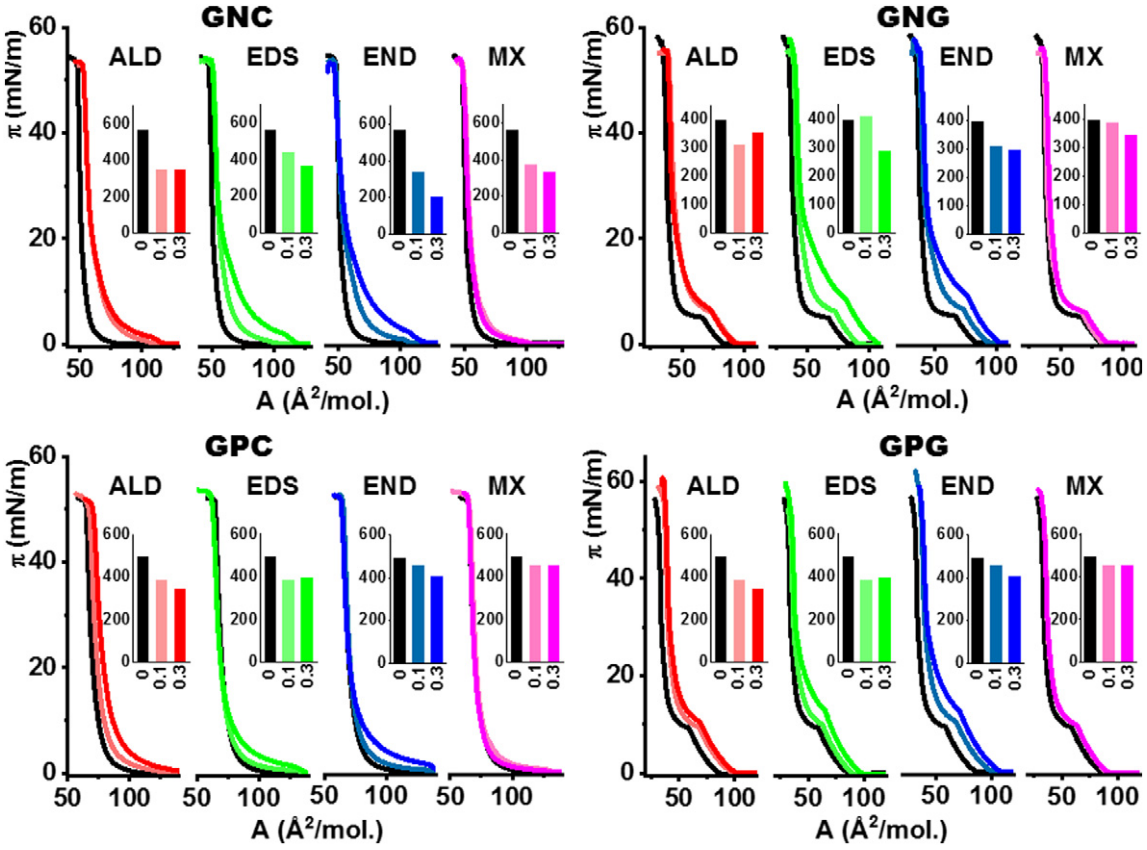

Fig. 1. π-A isotherms for the model membranes GNC, GNG, GPC and GPG doped with the investigated CP. Insets – maximal C_S^{-1} values for these monolayers (Y axis C_S^{-1}, X axis X(CP)).

applied in the GIXD experiments are described on the SOLEIL web site (www.synchrotron-soleil.fr). The detailed description of the experimental procedures and the elaboration of GIXD data can be found in our previous papers [43].

2.6. PM-IRRAS

KSV-NIMA PM-IRRAS spectrometer (PMI 550) was applied for these experiments. The spectral range of this instrument is 800–4000 cm^{-1} and the resolution 8 cm^{-1}. The FTIR spectrometer equipped with polarization modulation unit (ZnSe modulator PEM-100, Hinds Instruments, USA) is situated on one arm of the goniometer, whereas the MCT detector is situated on the other. The IR beam is directed out of the spectrometer to the Langmuir trough and reflected from the monolayer. The incident angle to the monolayer normal was 80° as at the grazing incidence angles the highest signal-to-noise ratio is achieved. The incoming light was continuously modulated between the p and s polarization, allowing simultaneous measurements of the spectra for both polarizations. The difference between the two signals gives surface-specific information and the sum provides the reference spectrum. The PEM-100 modulator operated at the 50 kHz frequency, the frequency of the highest amplification was set to 1500 cm^{-1} and the retardation was 0.5. The total acquisition time for each spectrum was 5 min, which is equivalent to 3000 interferograms (scans). The further details regarding the elaboration of the spectra can be found in the literature [44,45]. The FFT procedure was performed by the spectrometer software in the Mertz mode with the application of Blackman apodization function. The spectra were baseline corrected. The spectrometer and the Langmuir trough were placed on the optical table (Standa Ltd, Vilnius, Lithuania) equipped with active vibration isolation system (antivibration system VarioBasic 40, Halcyonics, Göttingen, Germany).

3. Results and discussion

At the first stage of the experiments the π-A isotherms for the model membranes were measured upon their compression. Due to the fact that CP are not surfactants or Langmuir-monolayer forming molecules we followed the idea to keep the number of phospholipid molecules constant in each experiment and increased the total number of molecules present at the interface adding the appropriate amount of CP solutions to achieve finally the mole ratios X(CP) of 0.1 and 0.3. In such established conditions the incorporation of CP between the phospholipid molecules means the increase of the number of molecules present directly in the monolayer; thus the isotherm should be switched toward larger mean molecular areas. On the other hand, if CP molecules are not incorporated into the model membrane the isotherms should remain unchanged regarding their course and location. The resultant π-A isotherms for the models GNC, GNG, GPC and GPG are presented in Fig. 1, whereas for BAC and BAG in SFig1 of the Supporting Materials. The compression moduli C_S^{-1} were calculated for all the monolayers and the maximal C_S^{-1} values are shown as column plots in insets of the panels of these figures.

The most significant shifts towards larger mean molecular area values are observed in the system GNC for all the investigated CP excluding MX. In the system GNC/ALD the isotherms at X(ALD) = 0.1 and 0.3 overlap completely, so it can be concluded that some ALD molecules were built into the monolayer but that the number of the incorporated molecules was independent on the declared X(ALD). The situation is different in the case of EDS and END as the isotherms shift successively toward greater A values with increasing X(CP), so it can be concluded that the number of CP molecules incorporated to the model membrane is proportional to X(CP). In the case of MX the isotherms are within the limit of experimental uncertainty identical to the π-A isotherm registered for the model membrane without the CP addition. This trend was identical for all the investigated systems, so it can be stated that MX do not incorporate into the model bacterial membranes. Similar trends were observed for the GNG model membrane doped with CP molecules; however, the shifts of the isotherms were less profound than in the mixtures with GNC. Regarding the GPC model it turned out that the shifts caused by the incorporation of CP were much less noticeable than in the GNC model membrane. More significant shifts were observed for the model GPG but also here the shifts are less profound than in the GNG model. So at first approximation it can be stated that CP molecules easier incorporate to the artificial Gram-negative than to the Gram-positive bacterial membranes. Following the courses of the π-A isotherms in all the four panels of Fig. 1 it can be observed that at higher surface pressures curves for the monolayers doped in CP approach these registered for the model bacterial membranes without the CP addition and in some cases overlap with them. Thus, it can be inferred that with the surface pressure rise at π > 20 mN/m the CP molecules can separate from the phospholipid matrix. Regarding the maximal

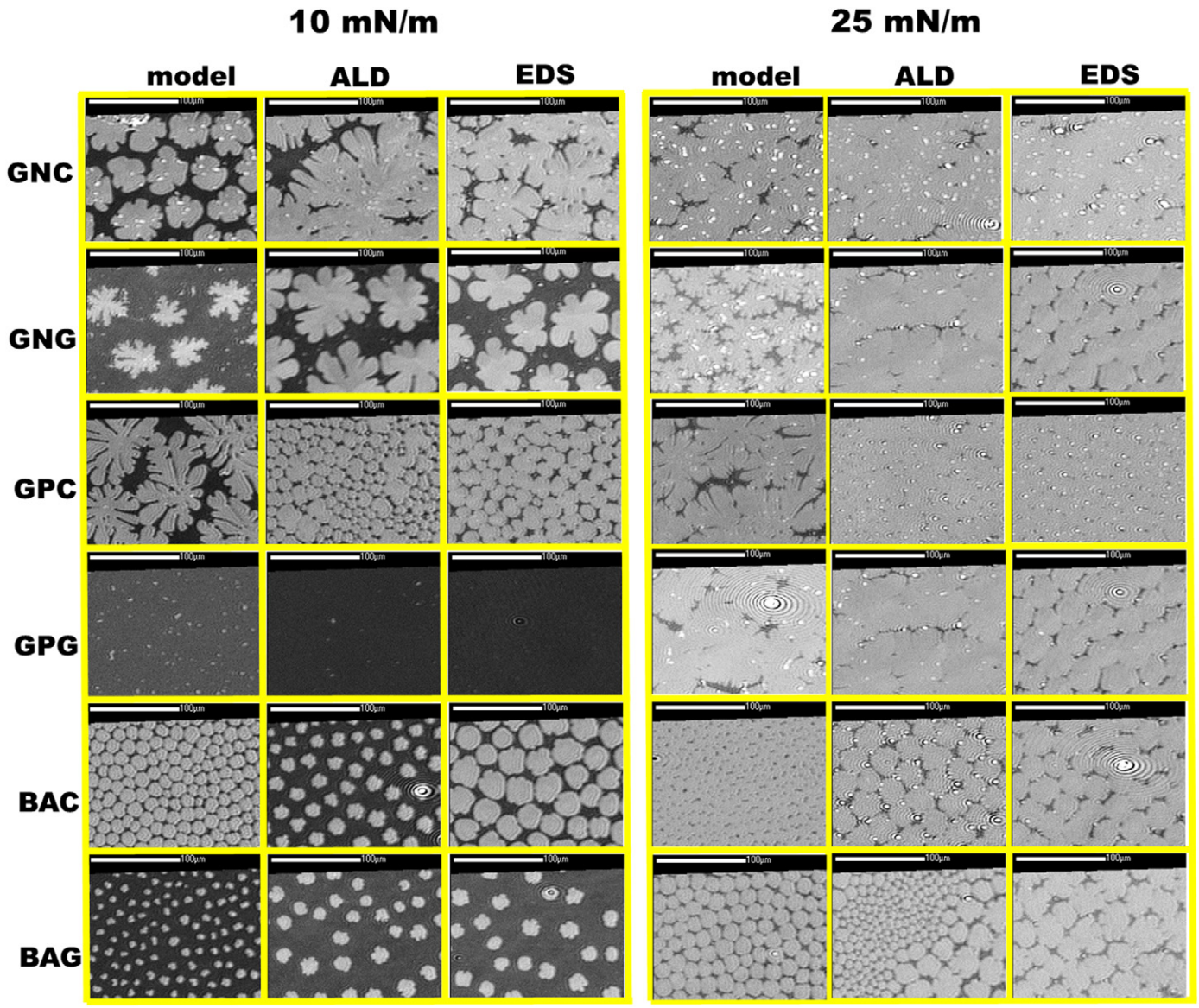

Fig. 2. Representative BAM images for the model membranes doped with ALD and EDS at X(CP) = 0.1. The scale bar in the photos indicates 100 μm.

C_S^{-1} values presented as column plots in the insets of the panels of Fig. 1. It can be stated that in most cases the presence of CP molecules within the model membranes increases its elasticity which results in the fall of C_{smax}^{-1} values. However, it should be underlined that all the monolayers achieve the highest degree of organization possible to a Langmuir monolayer – the solid state, also in the presence of CP molecules.

The evolution of the texture of the monolayers and the effects of the CP presence on the morphology of the condensed domains forming in the model membranes was studied with the application of Brewster angle microscopy. The detailed sets of the BAM images for all the four investigated CP and model membranes shown with the surface pressure step of 5 mN/m are gathered in SFig2 to Sfig6 of the Supporting materials. Interpreting the π-A isotherms gathered in Fig. 1 and the detailed sets of BAM images it can be stated that endosulfan and endrin exert very similar effects on the model membranes; therefore, in Fig. 2 the effects of only aldrin and endosulfan on the model membranes at two π values of 10 and 25 mN/m are shown.

The effects of the presence of CP in the model membrane are noticeable both at 10 and 30 mN/m for all the model membranes. At 10 mN/m the presence of ALD and EDS affects mainly the shape and the size of the liquid condensed (LC) domains. The changes are significant in the system GNC in which the average diameter of the dendritic LC domains grows from ca. 40 μm observed for the model membrane without CP addition to ca. 200 μm in the presence of ALD. These changes are lass pronounced in the GNG system but this trend is still preserved. The opposite tendency is observed for the GPC model, as without the CP addition large dendritic domains (100–200 μm in diameter) were observed, whereas in the presence of the pesticides they were transformed to small circular domains (diameter of ca. 5–10 μm). In the case of the BAC and BAG models of Gram positive bacteria the LC domains present at 10 mN/m were small and circular already without the CP addition. In the presence of CP the size of the LC domains increased from ca. 5 to 15–20 μm. At 30 mN/m in the presence of CP the monolayers were more homogeneous and the 3D aggregates visible for the GNC and GNG models disappeared. On the other hand, the BAC and BAG monolayers formed solely by the negatively charged phospholipids were not homogeneous at high surface pressures regardless the presence of CP, which was probably connected with the repulsion of the negatively charged heads of these molecules. However, in the presence of CP the average diameters of the LC domains were visibly larger. All these observations corroborate the conclusions drawn from the analysis of the π-A isotherms that aldrin, endrin and endosulfan can be effectively built into the model bacterial membranes and that at least some of these CP molecules remains in the membrane environment even at high surface pressures.

As it was frequently discussed in the scientific literature [46–48] BAM images provide the image of the model system in the mesoscale. The observation of the evolution of the monolayer texture following different stimuli can provide valuable information about the model system, but the information is still indirect regarding the organization of the film-forming molecules in the molecular scale. Thus, to obtain information regarding the phospholipid molecules in the Å scale the length of the incident light falling at the monolayer should be shortened from hundreds of nanometers (BAM) to Ångstroms (X-ray). The technique which often provides multitude of information about the packing of the molecules within the monolayer plane is Grazing incidence X-ray diffraction (GIXD). The only but cardinal condition to obtain the diffraction signal in this method is the periodical organization of the film-forming molecules within the monolayer plane [49,50]. All the applied here binary model bacterial membranes turned out to be 2D crystalline at 25/mN/m; thus, we followed the effects exerted on the 2D structure of the model films by the incorporation of CP. Taking under consideration the same arguments as in the case of the

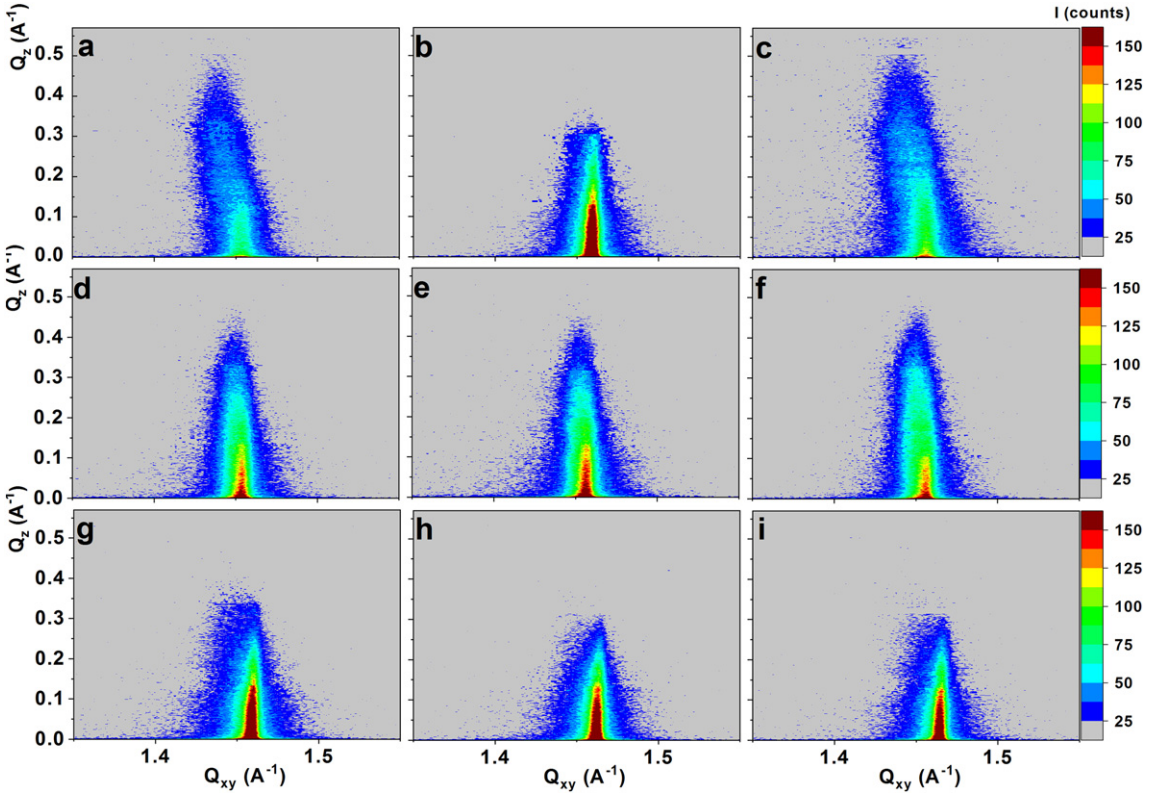

Fig. 3. GIXD intensity contour maps $I(Q_{xy},Q_z)$ for the following systems: a) GPG, b) GPG_ALD, c) GPG_EDS, d) GNG, e) GNG_ALD, f) GNG_EDS, g) BAG, h) BAG_ALD, i) BAG_EDS. X(ALD) = X (EDS) = 0.3, π = 25 mN/m.

BAM images the monolayers containing aldrin and endosulfan were compressed to 25 mN/m and subjected to the GIXD experiments. It turned out that for all the models containing cardiolipin only one symmetrical signal with its intensity maximum at $Q_z = 0$ Å^{-1} was observed meaning that the 2D crystal lattice was hexagonal regardless the presence of CP molecules at the air/water interface. The GIXD results for these systems were presented in SFig. 7 of the Supplementary materials. As it was proved in the mesoscale by BAM images greater effects of the CP molecules' presence were observed for the systems with DMPG: GPG, GNG and BAG; thus, we expected that also in GIXD results the 2D packing of the phospholipid molecules can be more susceptible to the presence of CP. The GIXD results for these model systems alone and doped by ALD and EDS at X(CP) = 0.3 are presented in Fig. 3.

It turned out that in four of the 9 above presented cases, that is: GPG, GPG_EDS, GNG_EDS and BAG the GIXD signal was a superposition of two independent signals: <0,2> with its intensity maximum at $Q_z = 0$ Å^{-1} and <-1,1> with its intensity maximum at $Q_z > 0$ Å^{-1}. In the interpretation of the intensity maps we followed the classical way [50,51] that is calculated the Bragg peaks $I(Q_{xy})$ integrated over the Q_z values and Bragg rods $I(Q_z)$ integrated over the Q_{xy} values. The plots of Bragg peaks and rods for these systems are presented in Fig. 4.

The important parameters extracted from the GIXD data are gathered in Table 2.

In the model membrane GPG containing 80% DMPG and 20% DMPE the scattering moieties, that is the myristic acid chains are tilted from the monolayer normal by the

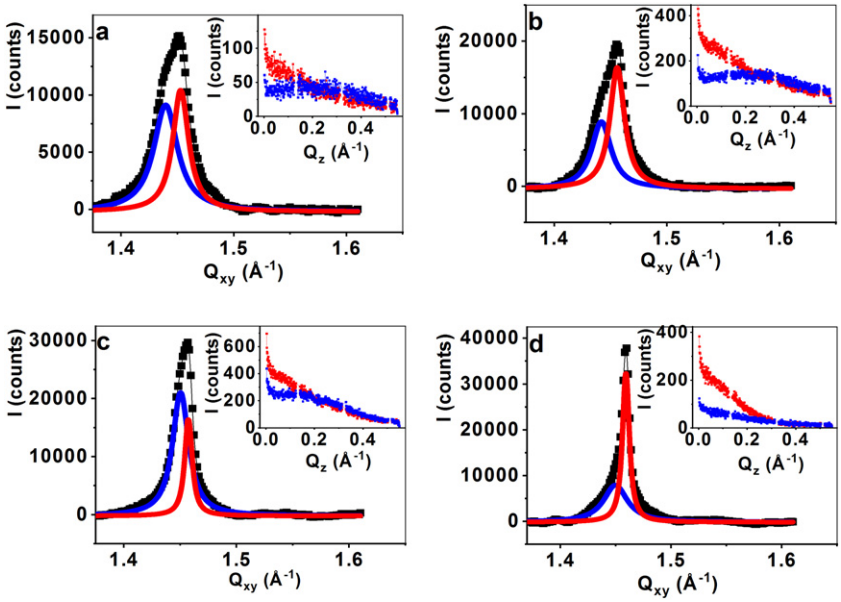

Fig. 4. Bragg peaks $I(Q_{xy})$ and Bragg rods $I(Q_z)$ (insets) for the following systems: a) GPG, b) GPG_EDS, c) GNG_EDS, d) BAG. The solid lines are Lorentz curves fitted to the experimental data: the blue to the <-1,1> signal and the red to the <0,2> signal. The same colors are applied in the plots of Bragg rods.

Table 2
Structural parameters extracted from the GIXD data.

Model	Q_{xy}, Q_z (Å^{-1}, Å^{-1})	a, b, γ (Å, Å, deg)	A (Å^2)	L_{xy} (Å)	τ (deg)
GPG	$_{<-1,1>}$ 1.439, 0.264 $_{<0,2>}$ 1.453, 0	5.058, 8.649, 90	43.7 (21.9 per chain)	$_{<-1,1>}$ 283 $_{<0,2>}$ 369	12.0
GPG_ALD	1.460, 0	a = b = 4.969, 120	21.4	601	0
GPG_EDS	$_{<-1,1>}$ 1.442, 0.24 $_{<0,2>}$ 1.456, 0	5.047, 8.631, 90	43.6 (21.8 per chain)	$_{<-1,1>}$ 263 $_{<0,2>}$ 352	11.2
GNG	1.452, 0	a = b = 4.997, 120	21.6	353	0
GNG_ALD	1.456, 0	a = b = 4.983, 120	21.5	395	0
GNG_EDS	$_{<-1,1>}$ 1.450, 0.140 $_{<0,2>}$ 1.457, 0	5.011, 8.625, 90	43.2 (21.6 per chain)	$_{<-1,1>}$ 325 $_{<0,2>}$ 718	6.4
BAG	$_{<-1,1>}$ 1.450, 0.110 $_{<0,2>}$ 1.460, 0	5.015, 8.606, 90	43.2 (21.6 per chain)	$_{<-1,1>}$ 213 $_{<0,2>}$ 783	5.0
BAG_ALD	1.463, 0	a = b = 4.959, 120	21.3	553	0
BAG_EDS	1.465, 0	a = b = 4.956, 120	21.3	576	0

angle of 12°. This leads to the appearance of two diffraction signals in the I(Q_{xy},Q_z) plot (Fig. 3 a) and the description of the 2D crystal lattice as rectangular centered [49,50]. The addition of aldrin to the model membrane withdraws the effect of the molecular tilt as at 25 mN/m the myristoyl chains were oriented upright at the air/water interface, which resulted in the hexagonal packing of the phospholipid molecules within the monolayer plain. This effect proves the presence of aldrin molecules built into the monolayer and the ordering and condensing effect exerted by this CP on the model membrane, that is conclusions, which were drawn from the mesoscopic scale BAM observations. The BAM images proved also that ALD and EDS exert similar effect on the GPG monolayer. On the contrary, the GIXD results discriminate over these CP, as EDS exerts virtually no effect on the organization of phospholipid molecules within the GPG monolayer, as the scattering moieties remained tilted and the reduction of the tilt from 12 to 11.2° was practically negligible. It would be reasonable to compare here the molecular scale GIXD results and the mesoscopic BAM images taken at 25 mN/m. As it is visible in Fig. 2 the GPG_ALD monolayer is homogeneous, whereas in the GPG_EDS film the condensed domains were separated from each other, so it can be stated that the GPG membrane doped by EDS was still in the LE/LC equilibrium. It is highly probable on the basis of the GIXD data that the EDS molecules were located in the LE phase, whereas they had no ability to be included into the 2D crystalline phospholipid nanodomains. Similar phenomena were observed also for the GNG model membrane composed in 70% of DMPE and 30% of DMPG. The monolayers doped by ALD differed from these doped by EDS in the BAM images as these with ALD were homogeneous at 25 mN/m and in these with EDS separate domains were observed. Regarding the 2D crystalline structure, the scattering moieties in the GNG model membrane were oriented perpendicularly in the monolayer plane which lead to the hexagonal packing of the scatterers. The addition of aldrin at X(ALD) = 0.3 do not disturb this ordering; whereas in the case of EDS the order of the myristoyl chains was disturbed and the small molecular tilt of 6.4° was observed, leading to the splitting of the diffraction signal. In the case of the BAG model membrane some small tilt of the myristoyl chains of 5° was identified. The addition of both ALD and EDS lead to the disappearance of the tilt and the perpendicular ordering of the scattering moieties. BAG is composed in 80% of DMPG, that is an anionic phospholipid and the tiny tilt of the hydrophobic chains can be caused by the repulsion of the negatively charged polar headgroups. The incorporation of some CP molecules between the hydrophobic chains of the phospholipid molecules can increase the intermolecular forces between the hydrophobic moieties and by this stabilize them in the upright orientation.

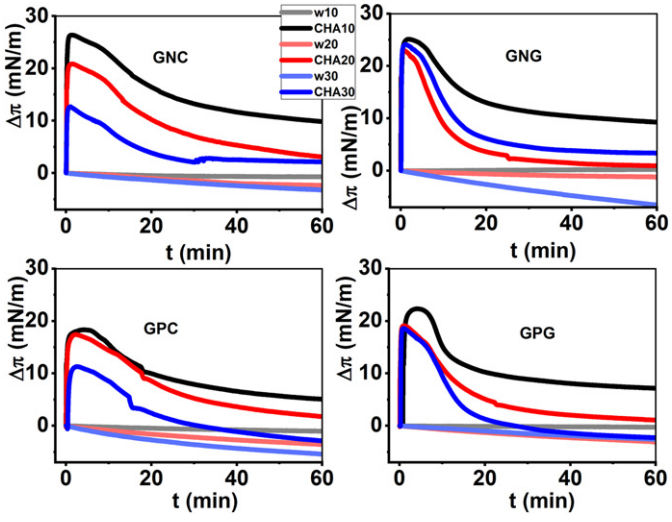

Fig. 5. Δπ – t plots registered in the penetration tests: black curve - initial π = 10 mN/m, red curve initial π = 20 mN/m and blue curve – initial π = 30 mN/m. The pale curves are the reference Δπ-t curves registered at the same initial π values without CHA injection.

3.1. The effect of soluble metabolite

Cyclodiene pesticides can; however slowly, be biodegraded in the soil. The degradation by anaerobic bacteria can lead to the common metabolite of all four investigated here CP a hexachloro, tricyclic dicarboxylic acid: 1,4,5,6,7,7-hexachloro-5-norbornene-2,3-dicarboxylic acid known in the industry also under the name chlorendic acid (CHA) [25,52]. This compound is also produced in large quantities and applied especially as a flame-retardant addition to plastics [26,28], so its presence in the environment can not only be connected with the CP degradation but also with the present applications of this compound. In contrast to the investigated here cyclodiene pesticides CHA is quite well water soluble; thus, its influence on the physical properties of the model bacterial membranes was investigated with the application of different techniques than in the first part of this article. To assess the susceptibility of a particular membrane model to the incorporation of CHA from the aqueous subphase the penetration tests were performed. The model membranes were compressed to a particular surface pressure value: 10, 20 or 30 mN/m, after which the mean molecular area was fixed and the monolayer was left for 20 min for relaxation. After this time the concentrated ethanol solution of CHA was injected deep into the well of the Langmuir trough and the temporal evolution of surface pressure was observed. To assess the effects of the monolayer relaxation we also performed the blank experiments on pure water without the CHA injection. The resultant data plotted as the Δπ – t curves are presented in Fig. 5. Δπ means here the difference between the initial π value at t_o (moment of CHA injection) and π noticed at a given t value.

For all the investigated monolayers the injection of the ethanolic solution of CHA into the subphase caused an abrupt increase of the measured surface pressure. It should be underlined here that the injection of 500 μl of pure ethanol had no effect on surface pressure for all the investigated systems, so the abrupt π increase is directly connected with the interaction of CHA with the model membranes. After the abrupt growth Δπ achieves its maximal value usually in the first 2–5 min after the CHA injection. Later on after a short (max 10 min) stabilization period the Δπ-t curve acquires a hyperbolic course, that is a relatively fast decrease region followed by a slow asymptotic decay. In the case of GNC the initial growth of Δπ depends significantly on the initial surface pressure value π_0. The largest Δπ of ca. 27 mN/m is observed at π_0 = 10 mN/m, whereas the smallest of 13 mN/m at π_0 = 30 mN/m. At π_0 = 10 mN/m Δπ aims to the asymptote of ca. 10 mN/m, which proves that multiple CHA molecules remain permanently built into the model membrane in such condition. For the initial π_0 value of 20 and 30 mN/m Δπ aims at the asymptotic value of ca. 2 mN/m meaning that the incorporation of CHA to the more condensed GNC monolayer is very limited. It should be underlined that the experiments are conducted in the conditions far from chemical equilibrium; therefore, initially just after the injection multiple CHA molecules gather in the electric double layer of the polar headgroups of the phospholipid molecules, some of which penetrate deep into the model membrane between the hydrophobic chains. However, with time elapse the systems strive to achieve the equilibrium and the excess CHA molecules are redistributed in the subphase. For us interesting is the final asymptotic Δπ value as it can be correlated with the number of CHA molecules permanently built into the model membranes. The GNG model membrane is less resistant to the CHA incorporation as the initial growth of π exceeds 20 mN/m regardless the π_0 value. Further on, the Δπ stabilizes at ca. 10 mN/m for π_0 = 10 mN/m and close to 0 for π_0 = 20 and 30 mN/m, so the courses of the Δπ-t curves indicate that with time elapse most CHA molecules detach the more condensed GNG monolayer. In the case of GPC and GPG the initial growth of π is comparable for both π_0 = 10 and 20 mN/m achieving the value of 18 mN/m, after which the temporal decay of Δπ starts, stabilizing at 5 mN/m for π_0 = 10 mN/m and 2 mN/m for π_0 = 20 mN/m. These values are smaller as observed in the case of the GNC model, which indicates that the applied models of Gram-positive bacteria membranes are quite more resistant to the incorporation of CHA from aqueous solution than their Gram-negative counterparts.

The model membranes were visualized by BAM upon the penetration experiments and the representative BAM images are gathered in Fig. 6.

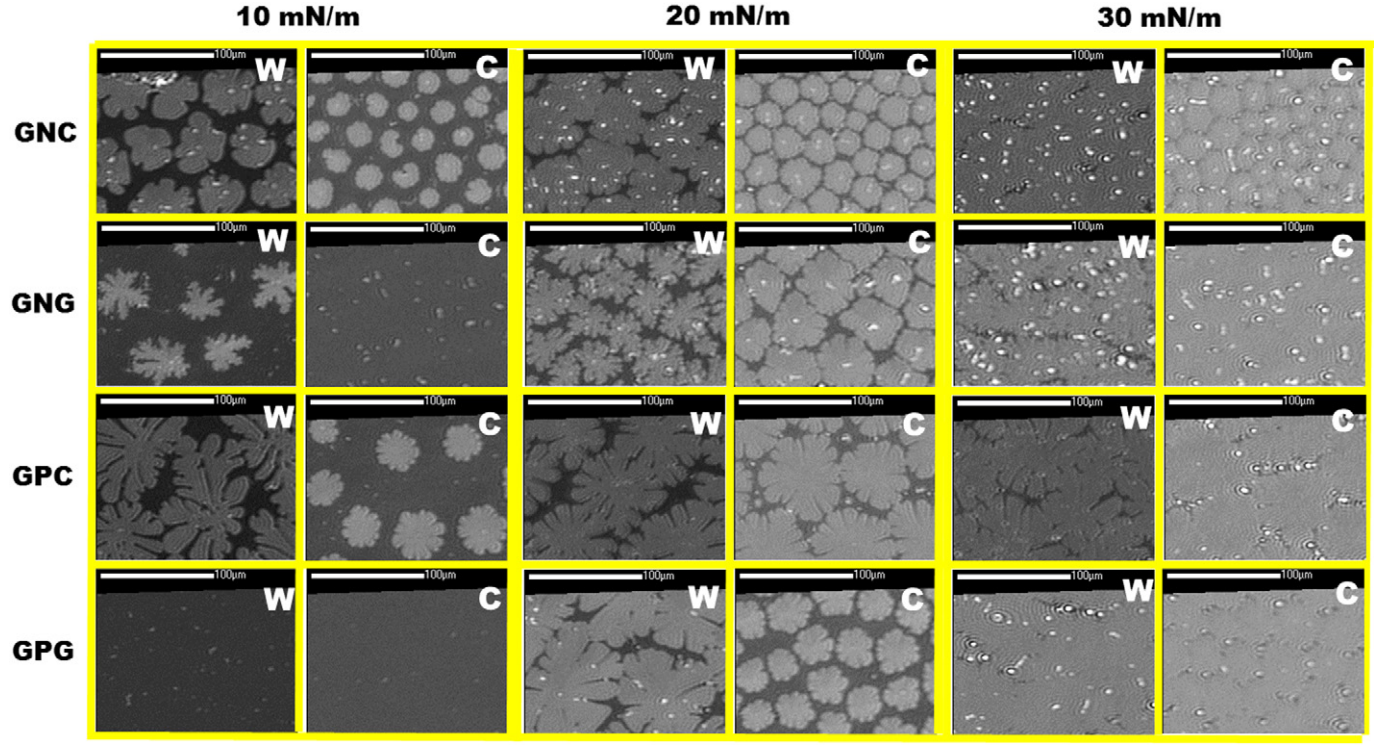

Fig. 6. Representative BAM images taken 60 min after the CHA injection. The photos taken on the subphase containing CHA (C) are compared with these taken on water (W).

At $\pi_0 = 10$ mN/m the effect of the presence of CHA in the subphase is significant for all the investigated model membranes. The most distinct differences can be observed for the GNG model, as on water condensed domains being in equilibrium with the LE phase can be observed while in the presence of CHA the domains fall apart and only the homogeneous LE phase can be observed. In the case of GNC the presence of CHA leads to the diminishing of the diameter of the condensed domains from ca. 40 μm–20 μm. It should also be underlined that the domains in the presence of CHA are more bright than on water. The gray level in BAM microscopy is connected with the thickness of the monolayer [46,47]. The thicker is the layer the more bright is the BAM image. Thus, it is proved by the BAM images that the incorporation of CHA molecules leads to the monolayer thickening. Different mechanisms can be responsible for this phenomenon. The location of CHA between the hydrophobic chains can lead to the increased undulation of the monolayer and the protrusion of some myristoyl chains. On the other hand the gathering of CHA in the vicinity of the polar headgroups can also lead to the net effect of the observed membrane thickening. In the case of the GPC model similar effects as for GNC can be observed, that is in the presence of CHA the condensed domains are smaller and brighter. The presence of CHA in the model membranes is also proved by BAM at the initial π_0 of 20 mN/m. The most significant effects can be observed for the GNC and GPG models as for them the domains are smaller and brighter than on water. For GNG and GPC the shapes of the domains are comparable both on water and on the CHA containing subphase, but these on CHA are brighter, indirectly proving the presence of some CHA molecules in the model membranes. In contrast to the data discussed so far, the BAM photos taken both on water and on the CHA solution 60 min after the beginning of the experiment at $\pi_0 =$ 30 mN/m are very comparable for all the investigated model membranes. This means that the presence of incorporated CHA molecules within the monolayer matrix is very limited or negligible.

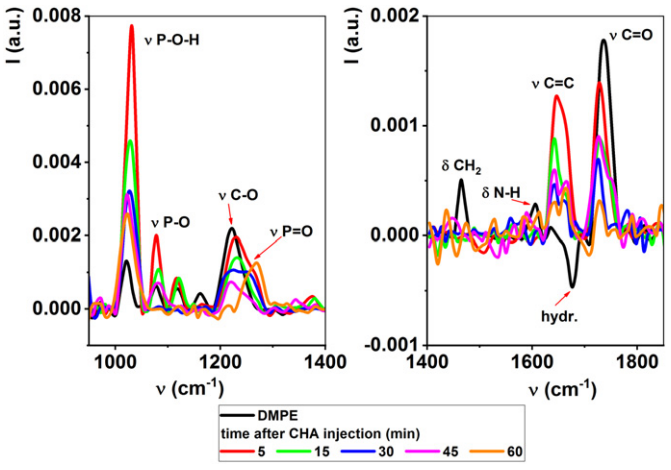

Fig. 7. PM-IRRAS results for the DMPE monolayer compressed to 20 mN/m before and after the CHA injection.

The interpretation of the penetration tests Δπ-t curves and the BAM images taken at these experiments leads to the conclusion that CHA molecules can interact both with the hydrophobic chains of the phospholipid molecules as well as with the headgroups and that significant replacements of the CHA molecules in the monolayers and in their close vicinity take place during the 1-h long experiments. Unfortunately, the headgroups of the monolayer-forming molecules are less accessible to most of the experimental techniques applied in the Langmuir monolayer studies than the hydrophobic chains. The technique which overcomes these limitations is for sure the surface-dedicated PM-IRRAS spectroscopy [45,53–55]. Thus, to have an insight in the interactions of the model systems with the CHA molecules this technique was applied also for these studies. As it was mentioned in the introduction, the model membranes were formed by DMPE, DMPG and TMCL; however, to avoid problems connected with the overlapping of the IR bands of the phospholipid molecules in the binary monolayers we applied simplified models, that is one component monolayers, composed either of DMPE or DMPG. The former can be treated as simplified Gram-negative bacterial membrane model, whereas the latter as the simplified model of Gram-positive bacteria membrane. The studies were performed at $\pi = 20$ mN/m as it was proved by the Δπ-t curves and BAM images that the CHA molecules were present within the model systems and the greater condensation of the monolayers at 20 than at 10 mN/m is beneficial for the quality of the PM-IRRAS signal. The spectrum was recorded before the CHA injection, 5 min after the injection (at the maximum of the Δπ-t curve) and later on with the step of 15 min. It turned out that the obtained results were qualitatively very similar both for DMPE and DMPG monolayers, so in the paper in Fig. 7 we present the spectra for DMPE and in SFig8 of the Supporting materials the results for DMPG.

In our studies we were interested in the conformation of the polar headgroup of the phospholipid molecule; therefore, we present here the spectra in the range 950–1850 cm^{-1} for which the most important bands typical to the functional groups present in the headgroup can be observed. For the DMPE monolayer spread on pure water the most intense bands are: the stretching of the single C–O bond of the ester group at 1220 cm^{-1}, the deforming vibration of the CH_2 group at 1465 cm^{-1}, the negative band connected with the hydration of the headgroup at 1675 cm^{-1} and the very strong ester carbonyl stretching at 1735 cm^{-1}. The minor but still observable bands were P–O–H vibration at 1020 cm^{-1} and the vibration of the single P–O bond of the phosphate group at 1080 cm^{-1} and the deforming amine N–H vibration at 1605 cm^{-1}. It should be underlined that the vibration of the P═O bond, which provides often a strong signal in the

phospholipid IR spectra at ca. 1260 cm^{-1} was inactive for the DMPE monolayer on pure water. This band is often convoluted with the C–O ester vibration located usually at ca. 1220 cm^{-1}; however, here the C–O band is symmetrical, so it originates purely from the C–O vibration. Thus, it can be inferred that the orientation of the P═O transition momentum was intermediate between the parallel and perpendicular to the monolayer which resulted in the lack of the P═O band in the spectrum [44]. The injection of CHA into the subphase leads to significant changes of the spectrum characteristics. First of all the most intense band becomes that connected with the P–O–H vibration located at 1020 cm^{-1}. This is a direct proof of the increased presence of CHA molecules in the proximity of DMPE polar headgroup. CHA is a dicarboxylic acid and its presence close to the phosphate group can lead to its significant protonation and the resultant 6-fold increase of the P–O–H band intensity as compared with the DMPE monolayer spread on pure water. The signal of the P–O group is also more intense meaning that the transition momentum is now closer to the parallel orientation resulting in the more intense positive band in the PM-IRRAS spectrum [44]. The wide intense band between 1200 and 1300 is not more symmetrical with a visible broadening at the larger υ values, which means that the transition momentum of the P═O group is now also closer to be parallel to the monolayer plane and the resultant signal is now the superposition of the ester C–O vibration and the P═O stretching. The band connected with the deforming CH_2 vibration at 1465 cm^{-1} disappears completely, which is also an important observation. Generally, the presence of a quite intense δ-CH_2 band proves the high organization of the hydrophobic chains and low share of the *gauche* defects [54]. The disappearance of this band proves the incorporation of the CHA molecules between the hydrophobic chains of the model membrane and the disorder caused to the myristoyl chains ordering by the presence of CHA molecules. The negative band at 1675 cm^{-1} ascribed by many authors to the oriented hydration water molecules [54] disappears proving the significant change of the closest proximity of the phospholipid polar headgroup. Instead a very intense C═C stretching band appears at 1645 cm^{-1}. Indeed, a double bond is present in one of the rings of the CHA molecule (see Scheme 1). As it was discussed earlier the experiment was far from the equilibrium and with time elapse the system strives to achieve it. Thus, further spectra were registered with the 15 min step: 15, 30, 45 and 60 min after the CHA injection. Regarding the evolution of the PM-IRRAS spectrum it can be observed that the intensity of the P–O–H band decreases successively with time elapse. The large intensity of this band in the spectrum measured just after the CHA injection was connected with the withdrawal of the phosphate group dissociation proving increased presence of CHA molecules in the proximity of the headgroup. The lowering of the P–O–H band intensity is connected with the increasing dissociation of the phosphate group which can be treater as a measure of the decrease of the local CHA concentration. This observation is important and is in agreement with the conclusions drawn from the Δπ-t curves regarding the equilibration of the investigated systems and the dissolution of the initially adsorbed CHA molecules back in the subphase. Regarding the intense band between 1200 and 1300 cm^{-1} with time elapse it becomes more asymmetrical having obviously two maxima at 1220 and 1250 cm^{-1}, as it is clearly visible in the spectrum measured 30 min after the CHA injection. Finally, in the last scan 60 min after the experiment start, the share of the 1220 cm^{-1} band is negligible and the peak intensity composes mainly of the 1260 cm^{-1} band. This progressing alteration proves the relocation of the CHA molecules in the proximity of the DMPE headgroup affecting its conformation. The transition momentum of the ester C–O group which was originally located in the monolayer plane has now an intermediate orientation close to the 45° angle leading to the significant loss of the intensity of the resultant band in the PM-IRRAS spectrum. On the contrary, the P═O transition momentum which had originally the intermediate orientation is now located in the monolayer plane resulting in an intense positive band. The δ CH_2 band was no observed in any of the successive spectra proving the presence of CHA molecules between the myristoyl chains and its disordering action. The very intense C═C band loses its intensity in the successive spectra proving the dissolution of the CHA molecules in the subphase. What is interesting in the spectra recorded 30, 45 and 60 min after CHA injection this band has two separate maxima at 1640 and 1660 cm^{-1}, whereas in the spectra taken 5 and 15 min after the CHA injection this band is asymmetrical suggesting the presence of a second maximum right from that present at 1640 cm^{-1}. This is an interesting result because the splitting of the C═C signal can be connected with different surroundings of this bond proving the presence of two populations of the CHA molecules. The first group are the CHA molecules present between the hydrophobic myristoyl chain, that is in the quasi-oil phase, while the second group are the CHA molecules close to the polar headgroup which can be treated as dissolved in an aqueous solution. Indeed, the closest surrounding of the two CHA molecular populations is so different that the splitting of the C═C band, which is the only band directly proving the presence of the CHA molecule at the interface, should be expected. Finally, the intensity of the ester carbonyl C═O band at 1735 cm^{-1} decreases in the successive spectra. This proves the replacements of the CHA molecules within the monolayer with time elapse. The interpretation of this band can be connected with the C═C band. With time elapse the intensity of the maximum at 1660 cm^{-1}, which can be ascribed to the C═C bond in the hydrocarbon environment, increases while the C═O band intensity decreases. It can be interpreted as follows: with time elapse multiple CHA molecules initially adsorbed to the model membrane dissolve in the subphase which is reflected in the lowering intensity of the P–O–H vibration band and the lowering intensity of the C═C band in aqueous environment at 1640 cm^{-1}. On the other hand the CHA molecules which were incorporated into the monolayer migrate deeper between the hydrocarbon chains. These molecules lose the contact with the phosphate group but their contact with the ester carbonyl group is progressively increased. This leads to the rearrangement of the headgroup and reorientation of the C═O transition momentum from parallel to the monolayer plane to a more inclined intermediate orientation.

4. Conclusions

In our studies we intended to shed new light on the interactions of cyclodiene pesticides with model bacterial membranes. Our results proved that all hexachlorinated pesticides: aldrin, endosulfan and endrin can incorporate into the modeled phospholipid matrix of bacterial membranes. Only the dodecachlorinated mirex was not membrane active which was probably connected with its structure differing profoundly from the other investigated CP. Endoslufan which was during decades treated as a less toxic and more environmentally benign pesticide behaved in our studies similarly to endrin, which was by many authors classified as a "super toxic" substance with its toxicity comparable with polychlorinated dioxins. The differences observed between aldrin and endosulfan can be explained mainly by the presence of electronegative sulfur and oxygen atoms present in the EDS molecule. These atoms generate dipole momentum in EDS which increases the possible interactions between this pesticide and the polar headgroup of the phospholipid molecules. From the applied membrane models these imitating Gram-negative bacteria membranes turned out to be more susceptible on CP incorporation. This can be connected with the protective role of the four-chained cardiolipin which was present in two of the applied models of Gram-positive bacteria: GPC and BAC. The penetration tests and PM-IRRAS measurements corroborated that the polar, water soluble CP metabolites produced in the environment by the hydrolytic anaerobic degradation of CP in the soils or delivered to the environment anthropogenically as chlorendic acid and other polychlorinated flame retardants can also be built into the decomposer membranes altering their morphology. The most important observation in the experiments with chlorendic acid was the discovery of two different CHA molecules populations: these interacting with the polar headgroup within the electrical double layer and those incorporated deep between the hydrophobic chains of the phospholipid molecules. The experiments proved that with time elapse the population of the molecules incorporated between the hydrocarbon chains increased proving the uptake of the toxic metabolites from the aqueous subphase by the model membranes.

Acknowledgements

This project was financed by the National Science Centre (No 2016/21/B/ST5/00245). We gratefully acknowledge SOLEIL for provision of synchrotron radiation facilities and we would like to thank Dr. Philippe Fontaine for assistance in using SIRIUS beamline.

Appendix A. Supplementary data

Supplementary data to this article can be found online at https://doi.org/10.1016/j.molliq.2019.112019.

References

[1] D. Rosner, G. Markowitz, Persistent Pollutants: a brief history of the discovery of the widespread toxicity of chlorinated hydrocarbons, Environ. Res. 120 (2013) 126–133.
[2] M.I. Pinto, H.D. Burrows, G. Sontag, C. Vale, J.P. Noronha, Priority pesticides in sediments of European coastal lagoons: a review, Mar. Pollut. Bull. 112 (2016) 6–16.
[3] E. Matsumoto, Y. Kawanaka, S.J. Yun, H. Oyaizu, Bioremediation of the organochlorine pesticides, dieldrin and endrin, and their occurrence in the environment, Appl. Microbiol. Biotechnol. 84 (2009) 205–216.
[4] G.A. Tolstikov, S.A. Ismailov, F.A. Gimalova, N.A. Ivanova, M.S. Miftakhov, Science-intensive utilization of environmentally harmful polychlorocarbons. Synthesis of biologically active cyclopentanoids from hexachlorocyclopentadiene, Russ. Chem. Bull., Int. Ed. 62 (2013) 226–234.
[5] A. Nestorovska-Krsteska, Z. Zdravkovski, Theoretical study of the diastereofacial isomers of aldrin and dieldrin, Int. J. Mol. Sci. 7 (2006) 35–46.
[6] N.K. Dharmarathne, J.C. Mackie, J. Lucas, E.M. Kennedy, M. Stockenhuber, Mechanisms of thermal decomposition of cyclodiene pesticides, identification and possible mitigation of their toxic products, Proc. Combust. Inst. 37 (2019) 1143–1150.
[7] R. Jayaraj, P. Megha, P. Sreedev, Organochlorine pesticides, their toxic effects on living organisms and their fate in the environment, Interdiscip. Toxicol. 9 (2016) 90–100.

[8] R. Carson, Silent Spring, Houghton Mifflin Company, Boston, 1962.
[9] M.T. Wan, J. Kuo, J. Pasternak, Residues of endosulfan and other selected organochlorine pesticides in farm areas of the lower Fraser Valley, British Columbia, Canada, J. Environ. Qual. 34 (2005) 1186–1193.
[10] C. Qu, S. Albanese, A. Lima, J. Li, A.L. Doherty, S. Qi, B. De Vivo, Residues of hexachlorobenzene and chlorinated cyclodiene pesticides in the soils of the Campanian Plain, southern Italy, Environ. Pollut. 231 (2017) 1497–1506.
[11] J.D. Sherman, Why chlordane and the cyclodiene pesticides must be banned worldwide, Environ. Epidemiol. Toxicol. 1 (1999) 132–147.
[12] F. Wania, D. Mackey, Tracking the distribution of persistent organic pollutants, Environ. Sci. Technol. 30 (1996) 390–396.
[13] chm.pops.int - Official Site of the Stockholm Convention, Updated2018.
[14] H. Hung, Ten years of global monitoring under the Stockholm convention on persistent organic pollutants (POPs): trends, sources and transport modeling, Environ. Pollut. 217 (2016) 1–3.
[15] J. Abraham, S. Silambarasan, Biomineralization and formulation of endosulfan degrading bacterial and fungal consortiums, Pestic. Biochem. Physiol. 116 (2014) 24–31.
[16] G. Ren, G. Zeng, L. Tang, J. Wang, J. Wan, Y. Liu, J. Yu, H. Yi, S. Ye, R. Deng, Sorption, transport and biodegradation – an insight into bioavailability of persistent organic pollutants in soil, Sci. Total Environ. 610–611 (2018) 1154–1163.
[17] M. Gavrilescu, M. Fate, Of pesticides in the environment and its bioremediation, Eng. Life Sci. 5 (2005) 497–526.
[18] S. Hussain, M. Arshad, M. Saleem, A. Khalid, Biodegradation of α- and β-endosulfan by soil bacteria, Biodegradation 18 (2007) 731–740.
[19] R. Kataoka, K. Takagi, Biodegradability and biodegradation pathways of endosulfanand endosulfan sulfate, Appl. Microbiol. Biotechnol. 97 (2013) 3285–3292.
[20] M. Kumar, V. Lakshmi, S. Khanna, Biodegradation and bioremediation of endosulfan contaminated soil, Bioresour. Technol. 99 (2008) 3116–3122.
[21] G. Odukkathil, N. Vasudevan, Enhanced biodegradation of endosulfan and its major metabolite endosulfate by a biosurfactant producing bacterium, J. Environ. Sci. Health B 48 (2013) 462–469.
[22] K. Bharati, S.R. Mohanty, V.R. Rao, T.K. Adhya, Effect of endosulfan on methane production from three tropical soils incubated under flooded condition, Bull. Environ. Contam. Toxicol. 63 (1999) 211–218.
[23] X. Sun, L. Zhu, J. Wang, J. Wang, B. Su, Z. Du, P. Guo, Effects of endosulfan on the populations of cultivable microorganisms and the diversity of bacterial community structure in brunisolic soil, Water Air Soil Pollut. 228 (2017) 169.
[24] J. Zhang, J. Qin, C. Zhao, C. Liu, H. Xie, S. Liang, Response of bacteria and fungi in soil microcosm under the presence of pesticide endosulfan, Water Air Soil Pollut. 226 (2015) 109.
[25] H. Zaffar, R. Ahmad, A. Pervez, T.A. Naqvi, A newly isolated Pseudomonas sp. can degrade endosulfan via hydrolytic pathway, Pestic. Biochem. Physiol. 152 (2018) 69–75.
[26] N.S. Shah, J.A. Khan, A.H. Al-Muhtaseb, M. Sayed, B. Murtaza, H.M. Khan, Synergistic effects of HSO_5^- in the gamma radiation driven process for the removal of chlorendic acid: a new alternative for water treatment, Chem. Eng. J. 306 (2016) 512–521.
[27] P. Bhatt, M.S. Kumar, S. Mudliar, T. Chakrabarti, Biodegradation of chlorinated compounds – a review, Crit. Rev. Environ. Sci. Technol. 57 (2007) 165–198.
[28] S.N. Zhou, S. Siddique, L. Lavoie, L. Takser, N. Abdelouahab, J. Zhu, Hexachloronorbornene-based flame retardants in humans: levels in maternal serum and milk, Environ. Int. 66 (2014) 11–17.
[29] R.A. Videira, M.M.C. Antunes-Madeira, V.M.C. Madeira, Perturbations induced by α- and β-endosulfan in lipid membranes: a DSC and fluorescence polarization study, Biochim. Biophys. Acta 1419 (1999) 151–163.
[30] L. Shen, F. Wania, Compilation, evaluation, and selection of physical-chemical property data for organochlorine pesticides, J. Chem. Eng. Data 50 (2005) 742–768.
[31] K. Johnsen, C.S. Jacobsen, V. Torsvik, J. Sorensen, Pesticide effects on bacterial diversity in agricultural soils- a review, Biol. Fertil. Soils 33 (2001) 443–453.
[32] A. Kallimanis, S. Frillingos, C. Drainas, A.I. Koukkou, Taxonomic identification, phenanthrene uptake activity, and membrane lipid alterations of the PAH degrading *Arthrobacter sp.* strain Sphe3, Appl. Microbiol. Biotechnol. 76 (2007) 709–717.
[33] F.P. Chavez, F. Gordillo, C.A. Jerez, Adaptive responses and cellular behavior of biphenyl-degrading bacteria toward polychlorinated biphenyls, Biotechnol. Adv. 24 (2006) 309–320.
[34] D. Zhang, L. Zhu, F. Li, Influences and mechanisms of surfactants on pyrene biodegradationbased on interactions of surfactant with a *Klebsiella oxytoca* strain, Bioresour. Technol. 142 (2013) 454–461.
[35] S. Liu, C. Guo, X. Liang, F. Wu, Z. Dang, Nonionic surfactants induced changes in cell characteristics and phenanthrene degradation ability of Sphingomonas sp. GY2B, Ecotoxicol. Environ. Saf. 129 (2016) 210–218.
[36] F. Deng, J. Sun, R. Dou, W. Deng, Y. Liu, C. Yang, Z. Dang, Mechanism of enhancing pyrene-degradation ability of bacteria by layer-by-layer assembly biomicrocapsules, Ecotoxicol. Environ. Saf. 181 (2019) 525–533.
[37] S. Zorádová-Murínová, H. Dudášová, L. Lukáčová, M. Čertík, K. Šilharová, B. Vrana, Adaptation mechanisms of bacteria during the degradation of polychlorinated biphenyls in the presence of natural and synthetic terpenes as potential degradation inducers, Appl. Microbiol. Biotechnol. 94 (2012) 1375–1385.
[38] R.F. Epand, P.B. Savage, R.M. Epand, Bacterial lipid composition and the antimicrobial efficacy of cationic steroid compounds (Ceragenins), Biochim. Biophys. Acta 1768 (2007) 2500–2509.
[39] W. Dowhan, A retrospective: use of Escherichia coli as a vehicle to study phospholipid synthesis and function, Biochim. Biophys. Acta 1831 (2013) 471–494.
[40] T.H.P. Nguyen, Y.T.H. Pham, S.H. Nguyen, V. Baulin, R.J. Croft, B. Phillips, R.J. Crawford, E.P. Ivanova, The bioeffects resulting from prokaryotic cells and yeast being exposed to an 18 GHz electromagnetic field, PLoS One 11 (2016), e0158135.
[41] M.C. Trombe, M.A. Laneelle, G. Laneelle, Lipid composition of aminopterin-resistant and sensitive strains of Streptococcus pneumoniae. Effect of aminopterin inhibition, Biochim. Biophys. Acta 574 (1979) 290–300.
[42] J.T. Davies, E.K. Rideal, Interfacial Phenomena, Academic Press, New York, 1961.
[43] A. Wójcik, P. Perczyk, P. Wydro, M. Broniatowski, Effects of water soluble perfluorinated pollutants on phospholipids in model soil decomposer membranes, Biochim. Biophys. Acta 1860 (2018) 2576–2587.
[44] D. Blaudez, J.M. Turlet, J. Dufourcq, D. Bard, T. Buffeteau, B. Desbat, Investigations at the air/water interface using polarization modulation IR spectroscopy, J. Chem. Soc., Faraday Trans. 92 (1996) 525–530.
[45] H. Nakahara, S. Lee, O. Shibata, Specific interaction restrains structural transitions of an amphiphilic peptide in pulmonary surfactant model systems: an in situ PM-IRRAS investigation, Biochim. Biophys. Acta 1798 (2010) 1263–1271.
[46] W. Daear, M. Mahadeo, E.J. Prenner, Applications of Brewster angle microscopy from biological materials to biological systems, Biochim. Biophys. Acta 1859 (2017) 1749–1766.
[47] K.J. Edler, T. Brennan, S.J. Roser, Formation of mesostructured thin films at the air/water interface, Thin Solid Films 495 (2006) 2–10.
[48] A.I. Buzin, G. Brezesinski, D.R. Tur, V.S. Papkov, A.V. Bakirov, S.N. Chvalun, Structural characterization of self-organized mono- and multilayers of poly[bis(2,2,3,3 tetrafluoropropoxy)phosphazene] at the air/water interface, Macromolecules 48 (2015) 3327–3336.
[49] J. Als-Nielsen, D. Jacquemain, K. Kjaer, F. Leveiller, M. Lahav, L. Leiserowitz, Principles and applications of grazing incidence X-ray and neutron scattering from ordered molecular monolayers at the air-water interface, Phys. Rep. 246 (1994) 251–313.
[50] K. Kjaer, Some simple ideas on X-ray reflection and grazing-incidence diffraction from thin surfactant films, Physica B 198 (1994) 100–109.
[51] V.M. Kaganer, G. Brezesinski, H. Möhwald, P.B. Howes, K. Kjaer, Positional order in Langmuir monolayers, Phys. Rev. Lett. 81 (1998) 5864–5867.
[52] P. Thangadurai, S. Suresh, Biodegradation of endosulfan by soil bacterial cultures, Int. Biodeterior. Biodegrad. 94 (2014) 38–47.
[53] Q. Huo, L. Dziri, B. Desbat, K.C. Russell, R.M. Leblanc, Polarization-modulated infrared reflection absorption spectroscopic studies of a hydrogen-bonding network at the air-water interface, J. Phys. Chem. B 103 (1999) 2929–2934.
[54] R. Mendelsohn, G. Mao, C.R. Flach, Infrared reflection–absorption spectroscopy: principles and applications to lipid–protein interaction in Langmuir films, Biochim. Biophys. Acta 1798 (2010) 788–800.
[55] T.F. Schmidt, L. Caseli, O.N. Oliveira Jr., R. Itri, Binding of methylene blue onto Langmuir monolayers representing cell membranes may explain its efficiency as photosensitizer in photodynamic therapy, Langmuir 31 (2015) 4205–4212.